Urea removal in reclaimed water used for ultrapure water production by spent coffee biochar/granular activated carbon activating peroxymonosulfate and peroxydisulfate

Xinbo Zhang[a,b,1], Yuanying Yang[a,b,1], Huu Hao Ngo[a,c,*], Wenshan Guo[a,c], Fengxia Sun[d], Xiao Wang[e], Jianqing Zhang[e], Tianwei Long[a,b]

[a] *Joint Research Centre for Protective Infrastructure Technology and Environmental Green Bioprocess, School of Environmental and Municipal Engineering, Tianjin Chengjian University, Tianjin 300384, China*

[b] *Tianjin Key Laboratory of Aquatic Science and Technology, Tianjin Chengjian University, Jinjing Road 26, Tianjin 300384, China*

[c] *Centre for Technology in Water and Wastewater, School of Civil and Environmental Engineering, University of Technology Sydney, Sydney, NSW 2007, Australia*

[d] *College of Resources and Environment, Shandong Agricultural University, Taian, 271000, China*

[e] *TG Hilyte Environment Technology (Beijing) Co., LTD., Beijing 100000, China*

[1] Equal contribution

* Correspondence authors: Email: ngohuuhao121@gmail.com (H. H. Ngo)

Abstract

This study evaluated the performance of spent coffee biochar (SCBC)/granular activated carbon (GAC) activating peroxymonosulfate (PMS) and peroxydisulfate (PDS) for urea degradation in reclaimed water used for ultrapure water production. Results showed that catalyst and oxidant wielded a great influence on urea removal. Of them, the GAC-PMS system could completely remove urea at the least oxidant (1 g/L) and catalyst dosage (0.2 g/L). GAC activating PMS mainly depended on graphite C structure and minor oxygen functional groups. However, the amounts of urea removed by 600BC-PMS and 900BC-PMS were 57% and 70%, respectively. In the PDS system, the urea removal through GAC-PDS could reach 90%, which mainly depends on the graphite C structure of GAC. Using the same conditions, the urea removal of 900BC-PDS was similar to GAC-PDS, so it has some potential as an alternative to commercial GAC.

Keywords: Biochar; granular activated carbon; persulfate activation; ultrapure water; urea

1. Introduction

The semiconductor industry consumes a lot of water, especially given the increasingly finite water resources that Earth has. Water restrictions and shortages have put great pressure on the semiconductor industry's future. At present, using reclaimed water as raw water is a practical strategy for providing abundant raw water resources and makes recycling of water more viable. However, compared with tap water, the organics content in reclaimed water is higher, and some small molecular organics such as urea can only be removed with difficulty through the existing ultrapure water (UPW)

system (Choi and Chung, 2019; Zhang et al., 2021). Therefore, removing urea from reclaimed water is essential for retaining a high quality UPW effluent.

Recently, advanced oxidation processes (AOPs) based on persulfate have garnered much scientific attention (Ding et al., 2021; Luo et al., 2018). However, the direct reaction of persulfate with most organics is relatively slow and needs to be activated (Shen et al., 2020). Common activation methods include photocatalytic (Shen et al., 2020), heating (Wang et al., 2021), transition metal and carbon-based materials (Dong et al., 2019; Liang et al., 2019). Of these, adding carbon-based materials does not require external energy while avoiding the harm of metal leaching is an effective activation method. Granular activated carbon (GAC) is regularly used in heterogeneous catalysis due to its large specific surface area (SSA) and porous structure (Jung et al., 2016). Furthermore, biochar (BC) obtained by pyrolysis of waste biomass has similar physicochemical properties, since it is both economical and environmentally friendly, and subsequently attracted much attention (Dong et al., 2017; Luo et al., 2020; Zhang et al., 2020a). However, it was found that the persulfate activation effect and mechanisms of GAC and BC were different (Liang et al., 2019), even for BCs prepared by different pyrolysis temperatures (Yu et al., 2020). Currently, it is still unclear what are the urea removal effect and mechanism when employing these carbon-based materials.

Persulfate includes peroxymonosulfate (PMS) and peroxydisulfate (PDS) which have symmetrical and asymmetrical structures, respectively. The structural differences between PDS and PMS mean that the activation pathways of both also vary (Lee et al., 2020). Researchers have pointed out that both the contaminants removal performance and reaction mechanism of PMS and PDS differ, even when using the same catalyst

(Ding et al., 2021). It was reported that the O−O bond energy of PMS was higher than that of PDS, so it could be more complicated to activate PMS using the same conditions (Huang et al., 2021).

Consequently, to demonstrate the effectiveness of urea removal with the carbon-based materials-persulfate system, the BC prepared by two pyrolysis temperatures and commercial GAC were selected. Specifically, the removal of urea and underlying mechanism were assessed for the PMS and PDS systems activated by these carbon-based materials, respectively. The main objective of this study was to evaluate urea removal ability and reaction mechanism of carbon-based materials-persulfate systems, and offer a theoretical basis for future practical application. The investigations were: (1) urea adsorption of three carbon-based materials; (2) urea removal performance by PDS/PMS systems; (3) the influences of each catalytic system and the optimal removal conditions; and (4) the activation mechanisms of each catalytic system.

2. Materials and methods

2.1. Materials

Urea (CH_4N_2O, 99%) was obtained from Shanghai Yuanye Bio-Technology Co., Ltd. (Shanghai, China). Peroxymonosulfate ($2KHSO_5•KHSO_4•K_2SO_4$, active oxygen 4.5%) and sodium persulfate ($Na_2S_2O_8$, 99%) were purchased from Shanghai Macklin Biochemical Share Co., Ltd. (Shanghai, China). GAC was bought from Tianjin Guangfu Technology Development Co., Ltd. (Tianjin, China).

The SCBC used in this study was prepared from spent coffee grounds, and the preparation method was as follows (Zhang et al., 2020b). Firstly, the collected spent coffee grounds were dried to a constant weight in an oven, and then calcined in a muffle

furnace. The pyrolysis temperatures were set at 600 °C and 900 °C under limited oxygen for 2 h, and the pyrolysis heating rate was 5 °C /min. The obtained black solids were SCBC prepared at different temperatures, recorded as 600BC and 900BC, respectively.

2.2. Characterizations

The surface functional groups and structures of carbon-based materials were detected by Fourier transform infrared (FTIR, Nicolet iS10, US) and Raman Spectral (Renishaw inVia, UK), respectively. The elements valence state changes occurring in carbon-based materials were revealed by X-ray photoelectron spectrometry (XPS, K-alpha, USA). The SSA and porosity of carbon-based materials were determined utilizing the Brunauer-Emmett-Teller (BET) method. As well, 1 g carbon-based materials and 20 ml deionized water were mixed at 150 rpm and 25 °C for 24 hours, and this helped to detect the pH and electrical conductance (EC) for suspension (Hu et al., 2020). Ash refers to the inorganics left after burning and was calculated by the mass loss after incineration at 800 °C for 4 hours (Hu et al., 2020). The ash content is expressed as:

$$\text{Ash content (\%)} = (m_1-m_2)/(m_3-m_2) \times 100 \quad (1)$$

Where, m_1 is the weight of the crucible and sample after pyrolysis, m_2 is the weight of the crucible and m_3 is the weight of the crucible and sample before pyrolysis.

2.3. Catalytic experiments

Specifically, the urea solution (1 mg/L) was prepared with UPW and 400 ml was poured into a 500 ml conical bottle. Secondly, the carbon-based material was added. After that, persulfate was added and placed in a shaker to react for 5 h at 180 rpm and temperature of 25 °C. The samples were filtered through a 0.45 μm polyether sulfone

(PES) membrane before detection. Different persulfate dosages (0.8, 1.0, 2.0, 4.0 and 6.0 g/L) were selected to determine the influence of persulfate dosage, when urea concentration (1 mg/L) and the dosage of carbon-based material (0.2 g/L) were constant. Similarly, the different carbon-based material dosages (0.05, 0.1, 0.2, 0.4 and 0.8 g/L) were chosen to demonstrate the impact of carbon-based material dosage. All experiments were done in triplicate.

2.4 Adsorption experiments

The adsorption experiments were carried out with three carbon-based materials at 25 °C. Specifically, the urea solution (1 mg/L) was prepared with UPW and 400 ml was poured into a 500 ml conical bottle. Following this, the carbon-based material was added and placed in a shaker to react for 5 h at 180 rpm. The samples were filtered through a 0.45 μm polyether sulfone (PES) membrane before detection. Different carbon-based material dosages (0.05, 0.1, 0.2, 0.4 and 0.8 g/L) were chosen to ascertain the influence of dosage. All experiments were conducted in triplicate.

2.5 Determination of urea concentration

The urea concentration was detected by the 2,3-Butanedione monoxime method. Specifically, 10 ml sample was added into the tube and diluted to 25 ml with UPW. Then, 1.0 ml 2,3-Butanedione monoxime (2%) and 2.0 ml of antipyrine (0.2%) were added. After blending, a boiling water bath was used for 50 minutes as part of the experiment and then cooled with tap water for about 2 minutes. Finally, samples were detected by UV-Vis spectrophotometer (Island Ferry, UV-2600) at 460 nm.

3. Results and discussion

3.1 Characteristics of carbon-based materials

The ash content and pH of 900BC were higher than that of 600BC (see Table 1), indicating that the higher pyrolysis temperature caused the higher ash content and pH value. This was due to the more inorganics retained in the BC at the higher pyrolysis temperature (Hu et al., 2020). As a result, base cation and carbonate concentrations in the BC increased, while acidic functional groups decomposed at high temperature and pH increased (Kwak et al., 2019). Furthermore, the pH value of GAC was higher than 600BC and 900BC, which indicated that GAC contained more alkaline groups. The EC of these carbon-based materials was in the 1.49 to 4.82 ms/cm range, from highest to lowest: GAC, 900BC, and 600BC. Compared with 600BC, the EC of 900BC increased significantly and this could be attributed to the rising pyrolysis temperature. The loss of volatile substances increased the content of salinity in the ash fraction (Cantrell et al., 2012; Stefaniuk and Oleszczuk, 2015). The EC of GAC was highest; therefore GAC suspension might have higher salinity and stronger conductivity than 600BC and 900BC.

Table 1 Physicochemical properties of 600BC, 900BC and GAC

Hu et al. (2020) found that the increase of thermal temperature enlarged the SSA and total pore volume of BC. The same results could be seen from Table 1. Clearly, the SSA and total pore volume of 900BC increased compared with 600BC, while the average pore size declined. Additionally, the SSA, total pore volume and average pore size of GAC were much higher than 600BC and 900BC. The N_2 adsorption/desorption isotherms of three carbon materials were presented in Fig. S4. 600BC and 900BC

conformed to type I isotherms, indicating that they were mainly composed of micropores (Dai et al., 2020; Kim and Ko, 2020). There were no obvious hysteresis loops, suggesting that 600BC and 900BC featured only limited mesoporosity (Rezma et al., 2017). From the pore distribution, the micropores of 900BC slightly increased compared with 600BC, resulting in a certain increment in the SSA and total pore volume. Conversely, GAC was suited to type IV isotherm, and a hysteresis loop appeared at P/P_0 from 0.4 to 0.6, suggesting there were both micropores and mesopores in GAC (Tian et al., 2018). The micropores and mesopores of GAC appeared to be much more numerous than BC. Therefore, GAC had a larger SSA and more porous structure than other two BCs, so it may provide more active centers to activate persulfate (Luo et al., 2020).

The peak at around 3424 cm^{-1} represented the stretching vibration of –OH (see supplementary material). The vibration intensity of three carbon-based materials from highest to lowest was 600BC, 900BC and GAC, indicating that the decomposition of -OH might be accompanied during the pyrolysis process (Zhou et al., 2021). The band at 2930 cm^{-1} corresponded to the antisymmetric stretching of $-CH_2$, which disappeared when the pyrolysis temperature was high, implying that most of the aliphatic compounds were converted into carbon dioxide and other gases (Hu et al., 2020). The peak at 1720 cm^{-1} was attributed to the stretching vibration of carboxyl C=O. During the high temperature pyrolysis process, the carboxyl C=O disappeared and the acidic functional groups decreased. The band at around 1628 cm^{-1} belonged to the stretching vibration of aromatic C=O. The peak intensity of 900BC was weaker than 600BC, which indicated that higher temperature reduced the carbonization caused by aromatic

cracking and improved the level of graphitization (Kim and Ko, 2020). Additionally, the band at 1398 cm^{-1}, 1063 cm^{-1} represented the vibration of C=C, C-O-C, respectively. Obviously, the functional groups of 600BC were more abundant than 900BC. For GAC, there was no obvious stretching vibration of carboxyl C=O, and the stretching vibration intensity of C=O was weaker than BCs, but C = C and C-O-C were stronger.

With respect to Raman spectra, two obvious peaks were observed for all carbon materials: D peak (around 1348 cm^{-1}) and G peak (about 1603 cm^{-1}), representing the degree of structural defects and graphitization of carbon materials, respectively. It can be inferred that these three materials have defective structure and graphite structure concurrently (Kim and Ko, 2020). Meanwhile, the 2D band at around 2700 cm^{-1} could display the degree of three-dimensional graphite orientation (Kim and Ko, 2020; Prado et al., 2019), indicating the few layers graphite structure of these carbon-based materials. The D peak of 600BC was wider than others, demonstrating that it had more defect structure and poorer crystallinity, which was well correlated with the EC results. Previous research did report the same results that the poorer structural order of carbon-based material might lead to a lower EC value (Prado et al., 2019). In addition, the I_D/I_G value can reflect the disorder degree of carbon material, while higher I_D/I_G ratio represents higher disorder (Forouzesh et al., 2019b). The I_D/I_G values of 600BC, 900BC and GAC were 3.49, 3.16 and 2.50, respectively. The value of BC was higher than GAC, which may be caused by high pyrolysis temperature (Zhou et al., 2020).

3.2 Adsorption of urea by different carbon-based materials

As can be seen from supplementary material, the adsorption of these carbon-based materials for urea was very limited. It was mainly due to the hydrophilic nature of urea, whereas BC and GAC were hydrophobic (Nguyen et al., 2021). With an increasing adsorbent dosage, the adsorption effect on urea did not improve significantly, which was not consistent with other analyses (Safwat and Matta, 2018). Safwat et al. (2018) found that GAC could adsorb about 30% urea (1000 mg/L) under alkaline conditions (pH =9). The reason for this phenomenon may be the considerable difference in the urea's initial concentrations. The mass transfer resistance between high urea concentration and carbon-based materials was slight, which may enable their adsorption effect to improve (Liu et al., 2013).

3.3 Urea removal by the PDS activation system

3.3.1 Urea removal performance

Results indicated that PDS alone can remove approximately 50% of urea (Fig. 1), indicating that persulfate anion can directly oxidized part of urea (see Eq. (2) (Choi and Chung, 2019). With the increment of PDS dosage, the urea removal efficiency improved slightly. However, with the PDS concentration rising from 0.8 g/L to 6 g/L, the urea removal rate only increased by 8%. This suggested that the addition of PDS alone was ineffective and uneconomic.

$$CO(NH_2)_2 + 7H_2O + 8Na_2S_2O_8 \rightarrow CO_2 + 2NO^{3-} + 16Na^+ + 16SO_4^{2-} + 18H^+ \quad (2)$$

As can be seen in Fig. 1, the urea removal was enhanced via adding carbon-based materials to activate PDS. The urea removal efficiency of PDS systems activated

through 600BC, 900BC and GAC can reach 74%, 73% and 80% respectively. When the PDS concentration was low (≤1 g/L), the GAC-PDS system can remove about 60% of urea, while the removal efficiencies of 600BC-PDS and 900BC-PDS were not ideal. It could be explained by the high EC value, which was beneficial to accelerate mass transfer. In addition, the large SSA and porous structure of GAC resulted in more active sites. As well, the poor urea removal efficiency of 900BC-PDS and 600BC-PDS systems may be due to the combined effect of three reasons, namely, the lack of active sites of BC, the low PDS concentration and the competition for PDS between BC and urea (Forouzesh et al., 2019b; Liang et al., 2019). With the same low PDS amount (0.8, 1 g/L), 900BC with higher SSA and pore volume, showed lower urea removal efficiency compared to 600BC. It can be explained from the following BC characteristics that the main factor affecting the catalytic performance of BC might be the oxygen functional group rather than SSA and pore volume (Liang et al., 2019). With the increase of PDS dosage, the three PDS systems' urea removal efficiency rose. When the PDS concentration was 2 g/L, the efficiency of 900BC-PDS system was the best (73%). When the PDS concentration was 4 g/L, the 600BC-PDS and GAC-PDS systems exhibited the highest removal efficiencies of 74% and 80%, respectively.

Fig. 1. Comparison of urea removal by the PDS catalytic systems ([Carbon-based materials] 0.2 g/L, [urea] 1 mg/L; C_0 represent the initial urea concentration (mg/L) in the solution; C_t represent the urea concentration (mg/L) in the solution after the degradation reaction.)

Thus, it can be inferred that the PDS dosage had a considerable effect on the carbon-based material-PDS catalytic system. A higher PDS concentration can noticeably enhance urea removal efficiency. However, when the PDS concentration

exceeded the optimal dosage, the urea degradation efficiency dropped. It might be that a high concentration of PDS can scavenge sulfate radical (see Eq. (3) (Wei et al., 2016)). In addition, excessive PDS might produce sulfate anion without activation, which compromises urea removal efficiency. Meanwhile, sulfate anion also inhibited the production of HO• (Hou et al., 2012).

$$S_2O_8^{2-} + SO_4^{-\bullet} \rightarrow S_2O_8^{-\bullet} + SO_4^{2-} \qquad (3)$$

Overall, by comparing the urea removal performance of three carbon-based materials-PDS systems, it emerges that the urea removal by 600BC-PDS and 900BC-PDS was equivalent to GAC-PDS in some cases. Therefore, BC is expected to be a good alternative to commercial GAC as a 'green' and economical carbon-based material for removing urea by a carbon-based material-PDS catalytic system.

3.3.2 Effect of carbon-based material dosage

As shown in Fig. 2, the urea removal efficiency of GAC and 600BC rose when the dosage increased. When the dosage GAC and 600BC was 0.8 g/L, the removal rate can reach 90% and 70%, respectively. Apparently, the dosage of carbon-based materials was also a decisive factor in the carbon-based materials-PDS catalytic system. Higher carbon-based materials dosage can provide more active sites for activated PDS (Wu et al., 2018). Compared with 600BC-PDS, the GAC-PDS system functioned better, which may be due to the higher EC value, larger SSA and pore volume of GAC. However, when the dosage of 900BC was 0.2 g/L, the urea removal rate at its best reached 73% and the urea removal rate fell when the dosage continued to increase. Similar to prior studies, it can be inferred that excessive catalysts competed with the generated radicals,

resulting in a decline in removal efficiency (Wu et al., 2019). Therefore, the desired dosage varied from different carbon-based materials, and needs to be determined.

Fig. 2. Effect of carbon-based material dosage on urea removal ([PDS] 2 g/L, [urea] 1 mg/L; C_0 represent the initial urea concentration (mg/L) in the solution; C_t represent the urea concentration (mg/L) in the solution after the degradation reaction.)

3.3.3 Urea removal mechanism of three carbon-based materials activating PDS systems

The FTIR spectra and XPS spectra of three carbon-based materials before and after urea degradation reaction was analyzed and compared to explore the possible activation mechanism (see Fig. S2). The peaks at around 3429 cm^{-1}, 2928 cm^{-1}, 1630 cm^{-1}, 1396 cm^{-1}, 1396 cm^{-1} and 1878 cm^{-1}, represented the stretching vibration of -OH, the antisymmetric stretching vibration of $-CH_2$, the stretching vibration of aromatic C=O, C=C, C-O-C and the bending of aromatic C-H, respectively. It can be seen that the peak vibration intensity of 900BC at around 3429 cm^{-1}, 1630 cm^{-1}, 1396 cm^{-1} decreased after the reaction. It was inferred that oxygen functional groups (-OH, C=O) might participate the catalytic reaction, and C=C was also beneficial to the catalytic reaction. The peak vibration intensity of 600BC at 3429 cm^{-1}, 1630 cm^{-1} was weakened. It was inferred that the main oxygen functional groups which played a crucial role in 600BC-PDS catalytic system, whereas the contribution of C = C may be limited.

From the FTIR spectra (see supplementary material), it was assumed that the oxygen functional groups and C=C structure of BC may be the active sites in the catalytic processes, which can provide electrons to PDS and activate it. For GAC, the peak vibration intensity at 2928 cm^{-1} was greatly improved, and a new peak appeared at

around 878 cm^{-1} after reaction, indicating that PDS might interact with GAC, causing the vibration of C-H (Forouzesh et al., 2019a). The peak at 1396 cm^{-1} was relatively stable, and the vibration intensity of the peak at around 3429 cm^{-1}, 1630 cm^{-1}, and 1064 cm^{-1} increased obviously. It was speculated that PDS could greatly influence the surface functional groups of GAC.

Fig. 3 exhibited the C1s and O1s XPS spectra of three carbon-based materials before and after the reaction. The peaks at 284.8 eV, 286.2 eV and 288.8 eV represented graphite C/C-C/C-H, C-O and C=O, respectively. It was obvious that the graphite C/C-C/C-H ratio of three carbon-based materials decreased after activating PDS, while the C-O and C=O increased. These results were considered that the framework (graphite C/C-C/C-H) and defect edges of carbon-based materials were oxidized, and the oxygen functional groups increased significantly (Ouyang et al., 2019).

Fig.3. (a) C1s high resolution scans of 600BC before and (b) after activating PDS; (c) O1s high resolution scans of 600BC before and after activating PDS; (d) C1s high resolution scans of 900BC before and (e) after activating PDS; (f) O1s high resolution scans of 900BC before and after activating PDS; (g) C1s high resolution scans of GAC before and (h) after activating PDS; (i) O1s high resolution scans of GAC before and after activating PDS.

The results revealed that the graphite C and defect structure of carbon-based materials were important factors in the PDS activation systems. Combined with the Raman spectrum, the defect in the GAC was the least among the three carbon-based materials, but its urea removal was the best. It was inferred that the PDS activation by GAC mainly depended on the graphite C structure. The defect of 600BC was the highest and its C1s XPS spectrum change was limited after reaction, which indicated

that the defect structure and framework exerted little effect on PDS activation. As for 900BC, the defect was the second-highest and the C1s XPS spectrum changed greatly after reaction, so it can be concluded that PDS activation may be the interaction of graphite C and defect structure.

Generally, the binding energy will shift to a higher value when the element loses electrons, contrarily to a lower value (Liu et al., 2014). The binding energy for O1s in 900BC shifted to a higher value after reaction, which demonstrated that some electrons are transferred from O to PDS in the catalysis process. It can be inferred that oxygen functional groups wielded a positive effect on the PDS activation in the 900BC-PDS system. However, the left shift of 600BC and GAC was less than 900BC, suggesting that the electron transfer of oxygen functional groups in them was less than 900BC. Combined with the previous FTIR spectra analysis, the peak intensity of the oxygen functional groups on 600BC fell significantly after the reaction, indicating that it had a certain effect on the PDS activation, but weaker than 900BC. The peak intensity of oxygen functional groups on GAC remained stable, which strongly suggested that oxygen functional groups had little effect in the GAC-PDS system.

Based on the above results and analysis, it can be stated here that the activation effect on PDS depended on the interaction of the graphite C structure, defect structure and functional groups (-OH, C=O, C=C) of carbon-based materials. In the 600BC-PDS system, the oxygen functional group (-OH, C=O) constituted the main factor for activating PDS, while the key function to activate PDS in the GAC-PDS system was the graphite C structure. In the 900BC-PDS system, oxygen functional group, C=C, graphite C and defect structure all had positive effects and able to activate PDS.

Therefore, the PDS activation by 900BC was the outcome of various important factors.

3.4 Urea removal by PMS activation system

3.4.1 Urea removal performance

As can be seen from Fig. 4, PMS alone had a limited effect on the removal of urea. When the PMS concentration was 0.8 g/L, the urea removal rate was only 24%. Similar to PDS, the urea removal efficiency revealed only limited improvement with the PMS dosage increase. Therefore, adding PMS alone to remove urea may be uneconomical.

Fig. 4. Comparison of urea removal by the PMS catalytic systems based on different activators ([Carbon-based materials] 0.2 g/L, urea 1 mg/L; C_0 represent the initial urea concentration (mg/L) in the solution; C_t represent the urea concentration (mg/L) in the solution after the degradation reaction.)

Clearly, the urea removal efficiency of PMS systems was quite different from PDS systems. Specifically, the urea removal rate of GAC-PMS was excellent in that it can reach 100%, which was much higher than 600BC and 900BC with the removal rates of 57% and 70%, respectively. When the PMS concentration was only 0.8 g/L, GAC can remove 95% of urea. When the PMS concentration increased to 1 g/L, the removal efficiency of GAC-PMS system can reach 100%. It may be that PMS has an asymmetric structure and is more easily activated (Shen et al., 2020). However, with the increase of PMS dosage, the urea degradation efficiency dropped, which was similar to the results for the PDS system. This was also caused by the excessive PMS concentration. Compared with other catalytic systems, urea removal by 600BC and 900BC was greatly diminished. When the PMS concentration was less than 2 g/L, 600BC and 900BC could not activate PMS. It resulted from the combined effect of three factors: poor activated

sites, insufficient oxidants and competition for PMS between BC and urea (Forouzesh et al., 2019b; Liang et al., 2019). Similarly, under the condition of the low PMS dosages (0.8, 1 g/L), 900BC removed less urea compared to 600BC. It can be inferred that when the PMS concentration was low, the defect structure played a more important role in the BC-PMS system for urea removal than the surface area and pore volume (Liang et al., 2019). The detailed analysis was shown in Section 3.4.3.

When the PMS dosage increased to 4 g/L, the removal efficiencies of 600BC and 900BC were 57% and 59%, respectively. With expanding the PMS dosage, the removal efficiency of 600BC-PMS worsened, and only reached 39% when the PMS concentration stood at 6 g/L. However, the removal efficiency of 900BC-PMS continued to climb, and able to reach 70% when the PMS concentration rose up to 6 g/L. Based on this, it can be stated that the PMS dosage was one of the important factors, and the best concentration for each carbon-based material was different. The results showed that the optimal PMS concentration was 4 g/L for 600BC as the activator and 1 g/L for GAC. For 900BC, the desired dosage of PMS needs to be investigated further, but too much oxidant would lead to a substantial increase in costs and secondary pollution. The ultimate objective was to achieve better removal with less catalyst and oxidant, such as the GAC-PMS system. Further study on the mechanism of GAC-PMS system is of great importance for remediation strategies. In general, the activation effect of GAC was excellent in the PMS catalytic system, whereas the effect of BC was limited. The ability of BC-PMS systems to remove urea was even worse than BC-PDS systems.

3.4.2 Effect of carbon-based material dosage

The dosage effect of three carbon-based materials on urea removal in the PMS system is shown in Fig. 5. The catalytic effect of GAC was the best, with the urea removal rate of 90% at the GAC dosage of only 0.05 g/L. With the increase of GAC dosage, the urea removal efficiency improved even further. When the GAC dosage reached 0.4 g/L, urea can be completely removed. 900BC had a similar trend but the removal rate was less than GAC. When the 900BC dosage was 0.8 g/L, the removal rate stood at 50%. These results may have been caused by the different EC values, SSA and pore volumes of GAC and biochar. In addition, the urea removal rate rose with the increase of 600BC dosage. The best removal rate can reach 50% at the 600BC dosage of 0.4 g/L. From the above results, it can be observed that the catalyst dosage was another important factor for PMS systems, and the increase of the catalyst dosage was more conducive to activating PMS. However, when the 600BC dosage rose to 0.8 g/L, instead, the urea removal rate waned, which indicated that the optimal dosage of each carbon-based material was different in the PMS system. It is therefore necessary to explore the best possible activation conditions of each material for practical application.

Fig.5. Effect of carbon-based material dosage on urea removal ([PMS] 2 g/L, [urea] 1 mg/L; C_0 represent the initial urea concentration (mg/L) in the solution; C_t represent the urea concentration (mg/L) in the solution after the degradation reaction.)

3.4.3 Urea removal mechanism of three carbon-based materials activating PMS systems

To further explore the mechanism of three carbon-based materials in PMS catalytic system, FTIR spectra and XPS spectra of the three materials before and after reaction in PMS system were measured (see Fig. S3). The peaks at 3437 cm^{-1}, 1628 cm^{-1} and 1097 cm^{-1} of 900BC remained relatively stable after reaction, whereas the peak vibration intensity at 2930 cm^{-1} increased and at 1398 cm^{-1} decreased. It was suggested that the oxygen functional groups have only a limited effect on the PMS activation process, while the C=C structure still participated in the catalytic reaction. The peaks of 600BC at 2930 cm^{-1} and 1398 cm^{-1} changed little, but the peak vibration intensity near 3437 cm^{-1} and 1628 cm^{-1} very evidently decreased. It was confirmed that -OH and C=O of 600BC participated in the catalytic system, but the contribution of C=C was slight. On the other hand, the peak at 1398 cm^{-1} of GAC changed little, but the peak vibration intensity increased at 3437 cm^{-1}, 12930 cm^{-1}, 1628 cm^{-1} and 1097 cm^{-1}, which was analogous to the GAC in the PDS system.

Fig. 6 (a), (c) and (e) represented the C1s spectra of 600BC, 900BC and GAC, respectively after reaction in the PMS system. As shown in Fig. 6, the trend regarding changes in 600BC and 900BC after activating PMS was analogous to activating PDS. Apparently, the C1s XPS spectrum of 600BC-PMS changed more compared with the 600BC-PDS system. It can be inferred that the defect structure had a certain effect on the PMS activation. As for 900BC, the ratio of the carbon structure descended significantly and the proportion of oxygen functional groups increased ascended, which indicated that the defect structure played a positive role. On the other hand, the graphite

C/C-C/C-H of GAC decreased by 3.6%, the ratio of C-O decreased by 1.4% and C=O increased by 5%. Unlike the GAC-PDS system, the ratio of graphite C/C-C/C-H went down slightly in the GAC-PMS system, indicating that the main function did not owe anything to the carbon framework or defect structure. Another difference was that the ratio of C=O increased while C-O decreased, alluding to the transformation of oxygen functional groups. It was speculated that C-O played a positive role.

Fig. 6 (b), (d), (f) depicted the O1s XPS spectra of three carbon-based materials. The shift of 600BC was not obvious, while the apparent left shift of 900BC and GAC can be observed. It was taken into account that the oxygen functional groups of GAC and 900BC had electron transfer during the PMS activation, while 600BC had no obvious electron transfer. Combined with the previous FTIR spectra analysis, it was speculated that the loss of oxygen functional groups of 600BC may not be caused by electron transfer to activate PMS. What was observed was that the peak intensity of oxygen functional groups on 900BC and GAC changed little, confirming that the loss of oxygen functional groups was less in the reaction. Combined with XPS spectra, it can be inferred that the oxygen functional groups of 900BC and GAC were involved in the PMS activation process.

Fig.6. (a) C1s and (b) O1s high resolution scans of 600BC after activating PMS; (c) C1s and (d) O1s high resolution scans of 900BC after activating PMS; (e) C1s and (f) O1s high resolution scans of GAC after activating PMS.

Based on the above results and analysis, it can be stated that the PMS activation through these materials was also the result of the interaction of graphite C, defect structure, C=C and functional groups (-OH, C=O, C-O-C). Concretely, the PMS

activation by 600BC mainly depended on its defect structure. The PMS activation by 900BC occurred chiefly through the interaction of C=C, graphite C, defect structure and minor oxygen functional groups. The activation of GAC was primarily due to its graphite C structure and minor oxygen functional groups. In general, the removal efficiency of BC-PMS was worse than BC-PDS, but the effect of GAC-PMS was better than GAC-PDS.

3.5. Feasibility analysis

Table 2 summarizes the urea removal effect by various catalytic systems. For the BC-persulfate system, the amount removed was approximately 70%. Obviously, the activation effect of 900BC was better than 600BC and required less oxidant dosage. It was presumed that BC prepared at high pyrolysis temperature might be more conducive to activate persulfate. Meanwhile the activation effect of BC-PDS was better than BC-PMS. Therefore, BC prepared at high pyrolysis temperature as catalyst and PDS as oxidant may favor catalytic reaction in the BC-persulfate system better. For the GAC-persulfate system, commercial GAC had a higher EC value, large SSA and pore volume, less ash content and rich oxygen functional groups. Therefore, the performance of GAC-persulfate in removing urea was superior to that of BC-persulfate. Furthermore, the effect of activating PMS by GAC was better than activating PDS. If GAC was chosen as the catalyst, PMS selected as the oxidant may lead to more encouraging outcomes.

Table 2 Overview of urea removal in various catalytic systems

Generally, urea removal by GAC-PMS system was the best because it is complete. The demand for oxidant and catalyst was the least so if this was introduced into the

actual UPW system, the best scheme currently would be the GAC-PMS system. Preparing spent coffee grounds biochar was easy to accomplish and did not demand any special treatment. The BC production costs were far lower than commercial GAC (Hu et al., 2020). It is necessary to modify biochar, such as increasing the EC value, SSA and pore volume, and explore its ideal operating conditions, so as to further improve the ability of BC to remove contaminants and make it a viable alternative to commercial GAC.

This study proved that using carbon-based materials to activate persulfate on urea removal was indeed feasible. However, more complex problems still need to be solved for large-scale practical applications, such as pollutants competing in real water, and ensuring the stability and regeneration of carbon-based materials.

4. Conclusion

In this study, urea removal by three carbon-based materials (600BC, 900BC and GAC) via activating persulfate systems was compared and explained. The adsorption effect of each material on low concentration urea was almost negligible. However, the urea removal rate was enhanced by the persulfate catalytic system when three carbon-based materials served as activators. Specifically, carbon-based catalysts and oxidants greatly enhanced urea removal efficiency. The 900BC was proved to be a viable alternative to commercial GAC in removing urea from reclaimed water for ultrapure water production process.

Acknowledgments

This research was supported by Tianjin Municipal Science and Technology Bureau of China (Project No. 18PTZWHZ00140, 20JCZDJC00380) and TG Hilyte Environment Technology (Beijing) Co., LTD. (Project No. M-P-0-181001-001).

As Huu Hao Ngo, a co-author on this paper is Editor of Bioresource Technology, he was blinded to this paper during review, and the paper was independently handled by Ashok Pandey as Editor.

E-supplementary data for this work can be found in e-version of this paper online.

References

1. Cantrell, K.B., Hunt, P.G., Uchimiya, M., Novak, J.M. and Ro, K.S. 2012. Impact of pyrolysis temperature and manure source on physicochemical characteristics of biochar. Bioresour. Technol. 107, 419-428.
2. Choi, J. and Chung, J. 2019. Evaluation of urea removal by persulfate with UV irradiation in an ultrapure water production system. Water Res. 158, 411-416.
3. Dai, L., Li, L., Zhu, W., Ma, H., Huang, H., Lu, Q., Yang, M. and Ran, Y. 2020. Post-engineering of biochar via thermal air treatment for highly efficient promotion of uranium(VI) adsorption. Bioresour. Technol. 298, 122576.
4. Ding, Y., Wang, X., Fu, L., Peng, X., Pan, C., Mao, Q., Wang, C. and Yan, J. 2021. Nonradicals induced degradation of organic pollutants by peroxydisulfate (PDS) and peroxymonosulfate (PMS): Recent advances and perspective. Sci. Total Environ. 765, 142794.

5. Dong, C.-D., Chen, C.-W. and Hung, C.-M. 2017. Synthesis of magnetic biochar from bamboo biomass to activate persulfate for the removal of polycyclic aromatic hydrocarbons in marine sediments. Bioresour. Technol. 245, 188-195.
6. Dong, C.-D., Chen, C.-W., Tsai, M.-L., Chang, J.-H., Lyu, S.-Y. and Hung, C.-M. 2019. Degradation of 4-nonylphenol in marine sediments by persulfate over magnetically modified biochars. Bioresour. Technol. 281, 143-148.
7. Forouzesh, M., Ebadi, A. and Aghaeinejad-Meybodi, A. 2019a. Degradation of metronidazole antibiotic in aqueous medium using activated carbon as a persulfate activator. Sep. Purif. Technol. 210, 145-151.
8. Forouzesh, M., Ebadi, A., Aghaeinejad-Meybodi, A. and Khoshbouy, R. 2019b. Transformation of persulfate to free sulfate radical over granular activated carbon: Effect of acidic oxygen functional groups. Chem. Eng. J. 374, 965-974.
9. Hou, L., Zhang, H. and Xue, X. 2012. Ultrasound enhanced heterogeneous activation of peroxydisulfate by magnetite catalyst for the degradation of tetracycline in water. Sep. Purif. Technol. 84, 147-152.
10. Hu, X., Zhang, X., Ngo, H.H., Guo, W., Wen, H., Li, C., Zhang, Y. and Ma, C. 2020. Comparison study on the ammonium adsorption of the biochars derived from different kinds of fruit peel. Sci. Total Environ. 707, 135544.
11. Huang, W., Xiao, S., Zhong, H., Yan, M. and Yang, X. 2021. Activation of persulfates by carbonaceous materials: A review. Chem. Eng. J. 418, 129297.
12. Jung, K.-W., Choi, B.H., Hwang, M.-J., Jeong, T.-U. and Ahn, K.-H. 2016. Fabrication of granular activated carbons derived from spent coffee grounds by

entrapment in calcium alginate beads for adsorption of acid orange 7 and methylene blue. Bioresour. Technol. 219, 185-195.

13. Kim, D.-G. and Ko, S.-O. 2020. Effects of thermal modification of a biochar on persulfate activation and mechanisms of catalytic degradation of a pharmaceutical. Chem. Eng. J. 399, 125377.
14. Kwak, J.-H., Islam, M.S., Wang, S., Messele, S.A., Naeth, M.A., El-Din, M.G. and Chang, S.X. 2019. Biochar properties and lead(II) adsorption capacity depend on feedstock type, pyrolysis temperature, and steam activation. Chemosphere 231, 393-404.
15. Lee, J., von Gunten, U. and Kim, J.-H. 2020. Persulfate-Based Advanced Oxidation: Critical Assessment of Opportunities and Roadblocks. Environ. Sci. Technol. 54(6), 3064-3081.
16. Liang, J., Xu, X., Qamar Zaman, W., Hu, X., Zhao, L., Qiu, H. and Cao, X. 2019. Different mechanisms between biochar and activated carbon for the persulfate catalytic degradation of sulfamethoxazole: Roles of radicals in solution or solid phase. Chem. Eng. J. 375, 121908.
17. Liu, J., Zou, S., Xiao, L. and Fan, J. 2014. Well-dispersed bimetallic nanoparticles confined in mesoporous metal oxides and their optimized catalytic activity for nitrobenzene hydrogenation. Catalysis Science & Technology 4(2), 441-446.
18. Liu, L., Lin, Y., Liu, Y., Zhu, H. and He, Q. 2013. Removal of Methylene Blue from Aqueous Solutions by Sewage Sludge Based Granular Activated Carbon: Adsorption Equilibrium, Kinetics, and Thermodynamics. J. Chem. Eng. Data

58(8), 2248-2253.

19. Luo, J., Bo, S., Qin, Y., An, Q., Xiao, Z. and Zhai, S. 2020. Transforming goat manure into surface-loaded cobalt/biochar as PMS activator for highly efficient ciprofloxacin degradation. Chem. Eng. J. 395, 125063.
20. Luo, J., Zhang, Q., Wu, L., Feng, Q., Fang, F., Xue, Z., Li, C. and Cao, J. 2018. Improving anaerobic fermentation of waste activated sludge using iron activated persulfate treatment. Bioresour. Technol. 268, 68-76.
21. Nguyen, C.H., Fu, C.-C., Chen, Z.-H., Tran, T.T.V., Liu, S.-H. and Juang, R.-S. 2021. Enhanced and selective adsorption of urea and creatinine on amine-functionalized mesoporous silica SBA-15 via hydrogen bonding. Microporous Mesoporous Mater. 311, 110733.
22. Ouyang, D., Chen, Y., Yan, J., Qian, L., Han, L. and Chen, M. 2019. Activation mechanism of peroxymonosulfate by biochar for catalytic degradation of 1,4-dioxane: Important role of biochar defect structures. Chem. Eng. J. 370, 614-624.
23. Prado, A., Berenguer, R. and Esteve-Núñez, A. 2019. Electroactive biochar outperforms highly conductive carbon materials for biodegrading pollutants by enhancing microbial extracellular electron transfer. Carbon 146, 597-609.
24. Rezma, S., Birot, M., Hafiane, A. and Deleuze, H. 2017. Physically activated microporous carbon from a new biomass source: Date palm petioles. C. R. Chim. 20(9), 881-887.
25. Safwat, S.M. and Matta, M.E. 2018. Adsorption of urea onto granular activated alumina: A comparative study with granular activated carbon. Journal of

Dispersion Science and Technology 39(12), 1699-1709.

26. Shen, Z., Zhou, H., Pan, Z., Guo, Y., Yuan, Y., Yao, G. and Lai, B. 2020. Degradation of atrazine by Bi2MoO6 activated peroxymonosulfate under visible light irradiation. J. Hazard. Mater., 123187.
27. Stefaniuk, M. and Oleszczuk, P. 2015. Characterization of biochars produced from residues from biogas production. J. Anal. Appl. Pyrolysis 115, 157-165.
28. Tian, W., Zhang, H., Sun, H., Tadé, M.O. and Wang, S. 2018. One-step synthesis of flour-derived functional nanocarbons with hierarchical pores for versatile environmental applications. Chem. Eng. J. 347, 432-439.
29. Wang, S., Meng, Q., Zhu, Q., Niu, Q., Yan, H., Li, K., Li, G., Li, X., Liu, H., Liu, Y. and Li, Q. 2021. Efficient decomposition of lignocellulose and improved composting performances driven by thermally activated persulfate based on metagenomics analysis. Sci. Total Environ. 794, 148530.
30. Wei, X., Gao, N., Li, C., Deng, Y., Zhou, S. and Li, L. 2016. Zero-valent iron (ZVI) activation of persulfate (PS) for oxidation of bentazon in water. Chem. Eng. J. 285, 660-670.
31. Wu, J., Wang, B., Blaney, L., Peng, G., Chen, P., Cui, Y., Deng, S., Wang, Y., Huang, J. and Yu, G. 2019. Degradation of sulfamethazine by persulfate activated with organo-montmorillonite supported nano-zero valent iron. Chem. Eng. J. 361, 99-108.
32. Wu, Y., Guo, J., Han, Y., Zhu, J., Zhou, L. and Lan, Y. 2018. Insights into the mechanism of persulfate activated by rice straw biochar for the degradation of aniline. Chemosphere 200, 373-379.

33. Yu, J., Tang, L., Pang, Y., Zeng, G., Feng, H., Zou, J., Wang, J., Feng, C., Zhu, X., Ouyang, X. and Tan, J. 2020. Hierarchical porous biochar from shrimp shell for persulfate activation: A two-electron transfer path and key impact factors. Applied Catalysis B: Environmental 260, 118160.

34. Zhang, R., Li, Y., Wang, Z., Tong, Y. and Sun, P. 2020. Biochar-activated peroxydisulfate as an effective process to eliminate pharmaceutical and metabolite in hydrolyzed urine. Water Res. 177, 115809.

35. Zhang, X., Yang, Y., Ngo, H.H., Guo, W., Wen, H., Wang, X., Zhang, J. and Long, T. 2021. A critical review on challenges and trend of ultrapure water production process. Sci. Total Environ. 785, 147254.

36. Zhang, X., Zhang, Y., Ngo, H.H., Guo, W., Wen, H., Zhang, D., Li, C., Qi, L., 2020. Characterization and sulfonamide antibiotics adsorption capacity of spent coffee grounds based biochar and hydrochar. Science of the Total Environment 716, 137015.

37. Zhou, X., Zeng, Z., Zeng, G., Lai, C., Xiao, R., Liu, S., Huang, D., Qin, L., Liu, X., Li, B., Yi, H., Fu, Y., Li, L. and Wang, Z. 2020. Persulfate activation by swine bone char-derived hierarchical porous carbon: Multiple mechanism system for organic pollutant degradation in aqueous media. Chem. Eng. J. 383, 123091.

38. Zhou, Y., Liu, G., Liu, J., Xiao, Y., Wang, T. and Xue, Y. 2021. Magnetic biochar prepared by electromagnetic induction pyrolysis of cellulose: Biochar characterization, mechanism of magnetization and adsorption removal of chromium (VI) from aqueous solution. Bioresour. Technol. 337, 125429.

Figure Captions

Fig.1. Comparison of urea removal by the PDS catalytic systems ([Carbon-based materials] 0.2 g/L, [urea] 1 mg/L; C_0 represent the initial urea concentration (mg/L) in the solution; C_t represent the urea concentration (mg/L) in the solution after the degradation reaction.)

Fig.2. Effect of carbon-based material dosage on urea removal ([PDS] 2 g/L, [urea] 1 mg/L; C_0 represent the initial urea concentration (mg/L) in the solution; C_t represent the urea concentration (mg/L) in the solution after the degradation reaction.)

Fig.3. (a) C1s high resolution scans of 600BC before and (b) after activating PDS; (c) O1s high resolution scans of 600BC before and after activating PDS; (d) C1s high resolution scans of 900BC before and (e) after activating PDS; (f) O1s high resolution scans of 900BC before and after activating PDS; (g) C1s high resolution scans of GAC before and (h) after activating PDS; (i) O1s high resolution scans of GAC before and after activating PDS.

Fig.4. Comparison of urea removal by the PMS catalytic systems based on different activators ([Carbon-based materials] 0.2 g/L, urea 1 mg/L; C_0 represent the initial urea concentration (mg/L) in the solution; C_t represent the urea concentration (mg/L) in the solution after the degradation reaction)

Fig.5. Effect of carbon-based material dosage on urea removal ([PMS] 2 g/L, [urea] 1 mg/L; C_0 represent the initial urea concentration (mg/L) in the solution; C_t represent the urea concentration (mg/L) in the solution after the degradation reaction.)

Fig.6. (a) C1s and (b) O1s high resolution scans of 600BC after activating PMS; (c) C1s and (d) O1s high resolution scans of 900BC after activating PMS; (e) C1s and (f) O1s high resolution scans of GAC after activating PMS.

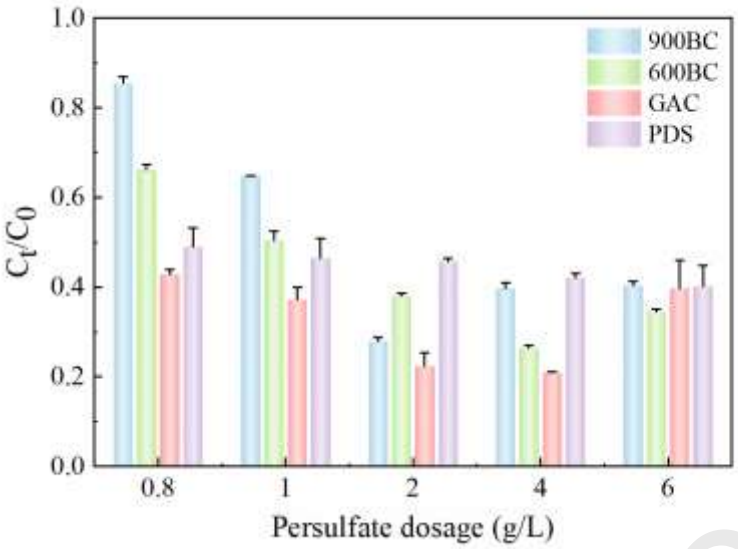

Fig.1. Comparison of urea removal by the PDS catalytic systems ([Carbon-based materials] 0.2 g/L, [urea] 1 mg/L; C_0 represent the initial urea concentration (mg/L) in the solution; C_t represent the urea concentration (mg/L) in the solution after the degradation reaction.)

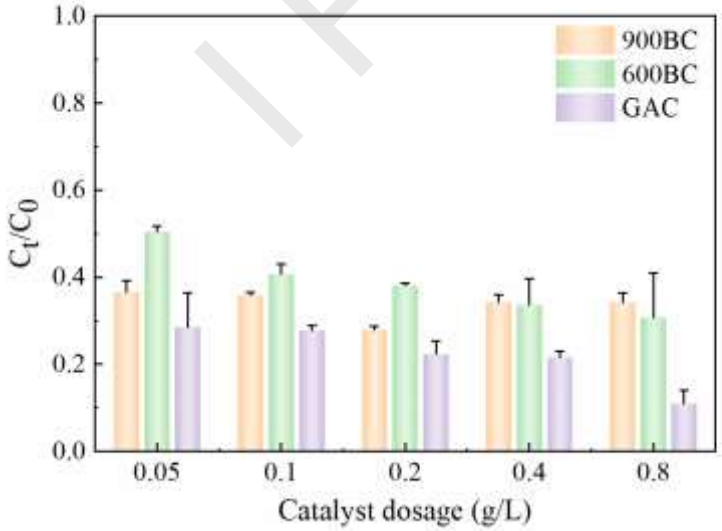

Fig.2. Effect of carbon-based material dosage on urea removal ([PDS] 2 g/L, [urea] 1 mg/L; C_0 represent the initial urea concentration (mg/L) in the solution; C_t represent the urea concentration (mg/L) in the solution after the degradation reaction.)

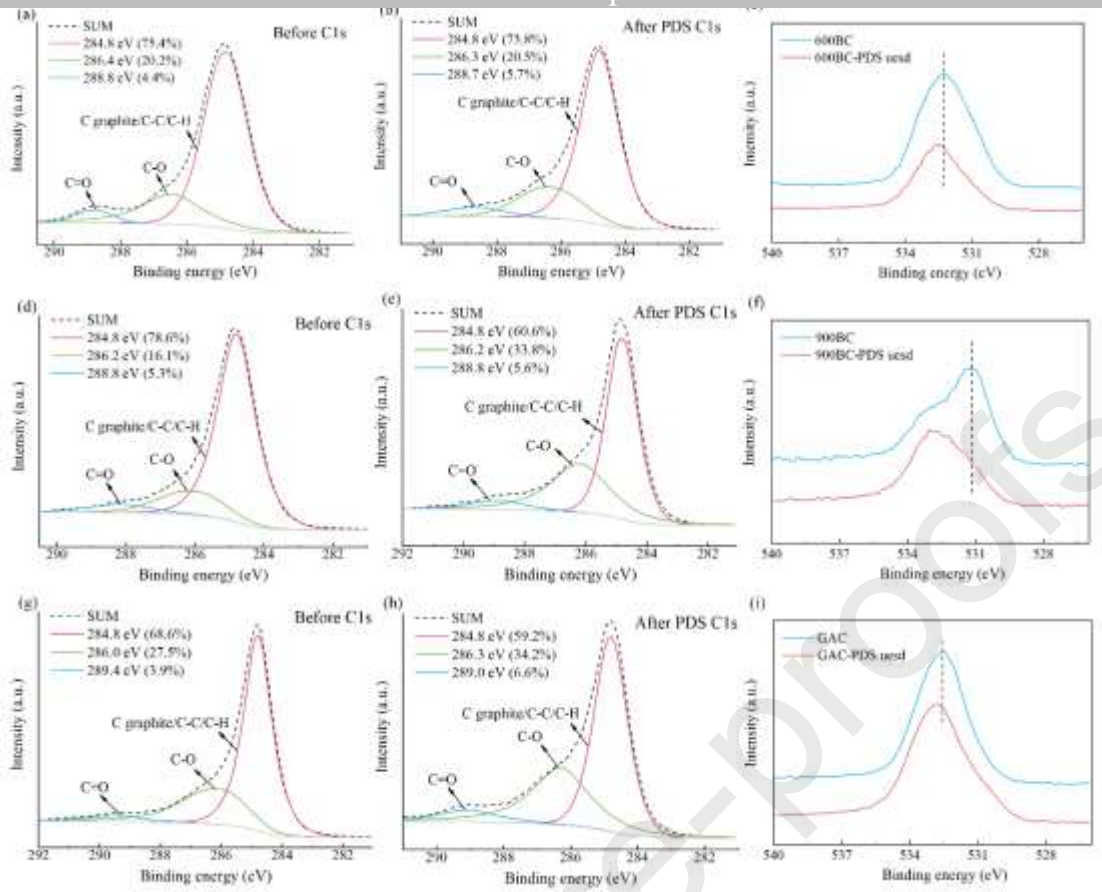

Fig.3. (a) C1s high resolution scans of 600BC before and (b) after activating PDS; (c) O1s high resolution scans of 600BC before and after activating PDS; (d) C1s high resolution scans of 900BC before and (e) after activating PDS; (f) O1s high resolution scans of 900BC before and after activating PDS; (g) C1s high resolution scans of GAC before and (h) after activating PDS; (i) O1s high resolution scans of GAC before and after activating PDS.

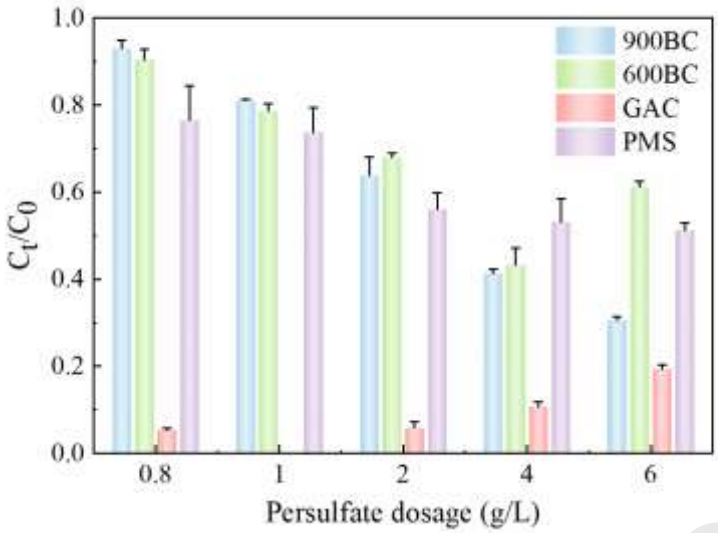

Fig.4. Comparison of urea removal by the PMS catalytic systems based on different activators ([Carbon-based materials] 0.2 g/L, urea 1 mg/L; C_0 represent the initial urea concentration (mg/L) in the solution; C_t represent the urea concentration (mg/L) in the solution after the degradation reaction)

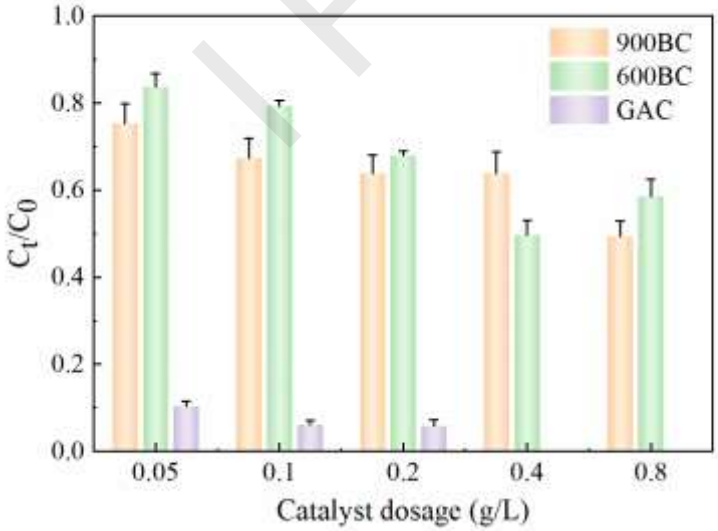

Fig.5. Effect of carbon-based material dosage on urea removal ([PMS] 2 g/L, [urea] 1 mg/L; C_0 represent the initial urea concentration (mg/L) in the solution; C_t represent the urea concentration (mg/L) in the solution after the degradation reaction.)

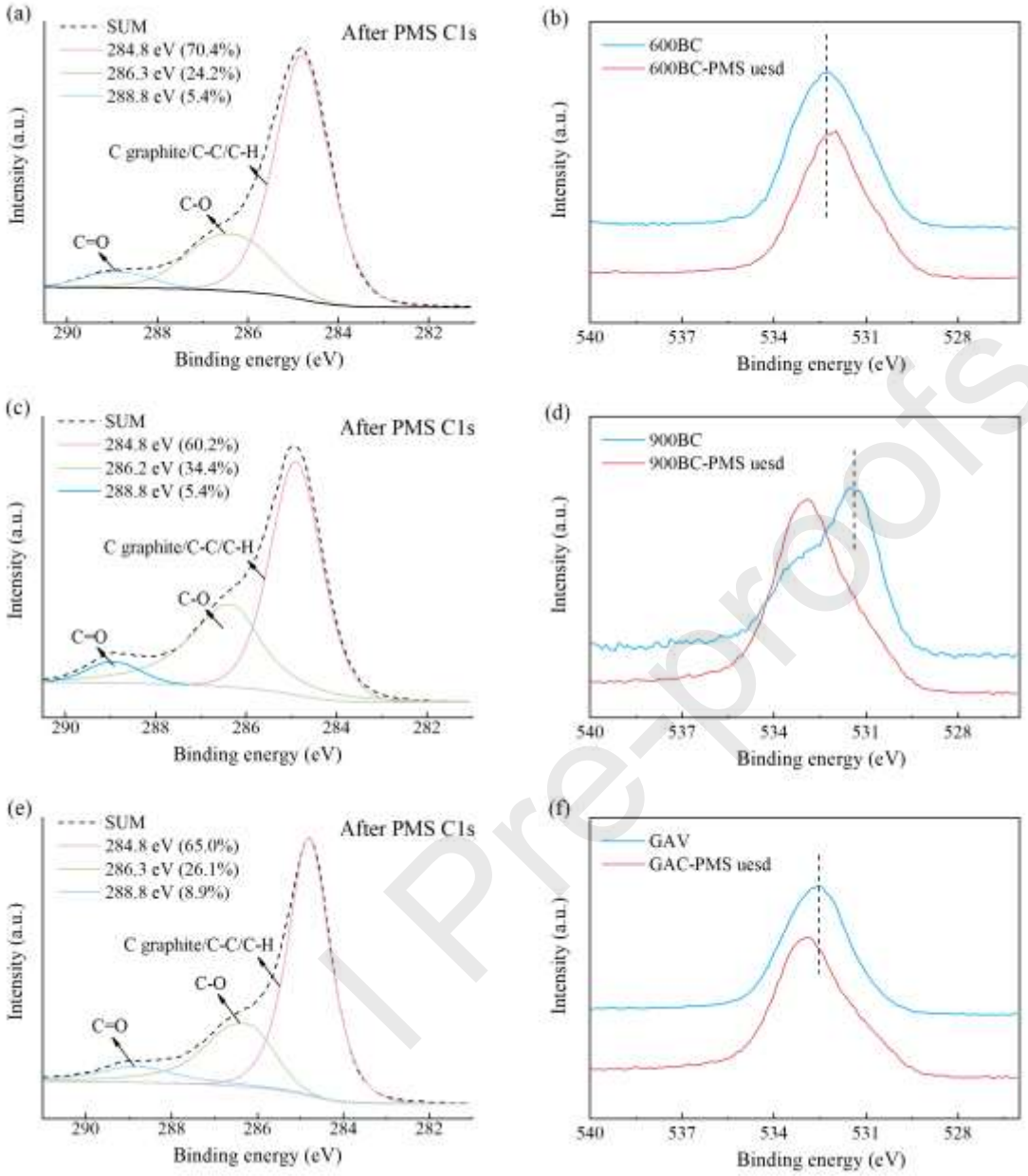

Fig.6. (a) C1s and (b) O1s high resolution scans of 600BC after activating PMS; (c) C1s and (d) O1s high resolution scans of 900BC after activating PMS; (e) C1s and (f) O1s high resolution scans of GAC after activating PMS.

Table 1 Physicochemical properties of 600BC, 900BC and GAC

Sample	pH	EC (ms/cm)	Ash (%)	Surface area (m^2/g)	Pore volume (cm^3/g)	Pore diameter (nm)
600BC	8.92±0.01	1.49±0.006	6.34±0.15	89.55	0.0168	2.98
900BC	9.93±0.01	2.65±0.007	7.72±0.13	99.19	0.0183	2.95
GAC	10.29±0.01	4.82±0.003	2.00±0.10	354.16	0.3300	4.74

Table 2 Overview of urea removal in various catalytic systems

Sample	Oxidant	Best urea removal efficiency (%)	Oxidant dosage (g/L)	Catalyst dosage (g/L)
600BC	PDS	74	4	0.2
600BC	PMS	57	4	0.2
900BC	PDS	73	2	0.2
900BC	PMS	70	6	0.2
GAC	PDS	90	2	0.8
GAC	PMS	100	1	0.2